

Magnetic Coupling and Single-Ion Anisotropy in Surface-Supported Mn-based Metal-Organic Networks

L. Giovanelli,¹ A. Savoyant,¹ M. Abel,¹ F. Maccherozzi,² Y. Ksari,¹ M. Koudia,¹ R. Hayn,¹ F. Choueikani,³ E. Otero,³ P. Ohresser,³ J.-M. Themlin,¹ S. S. Dhesi,² and S. Clair¹

¹*Aix-Marseille Université, CNRS, IM2NP UMR 7334, F-13397 Marseille, France*

²*Diamond Light Source, Didcot, OX11 0DE, United Kingdom*

³*Synchrotron SOLEIL, L'orme des Merisiers, Saint-Aubin - BP48, 91192 Gif-sur-Yvette CEDEX, France*

(Dated: February 10, 2022)

The electronic and magnetic properties of Mn coordinated to 1,2,4,5-tetracyanobenzene (TCNB) in the Mn-TCNB 2D metal-ligand networks have been investigated by combining scanning tunneling microscopy and X-ray magnetic circular dichroism (XMCD) performed at low temperature (3 K). When formed on Au(111) and Ag(111) substrates the Mn-TCNB networks display similar geometric structures. Magnetization curves reveal ferromagnetic (FM) coupling of the Mn sites with similar single-ion anisotropy energies, but different coupling constants. Low-temperature XMCD spectra show that the local environment of the Mn centers differs appreciably for the two substrates. Multiplet structure calculations were used to derive the corresponding ligand field parameters confirming an in-plane uniaxial anisotropy. The observed interatomic coupling is discussed in terms of superexchange as well as substrate-mediated magnetic interactions.

INTRODUCTION

Exploiting the functionality of organic molecules to manipulate electron spin has been the subject of intense scientific activity over the last few years [1–3]. The discovery of single molecule magnets displaying high blocking temperatures and quantum tunneling of magnetization suggested an alternative way to downsizing information storage [1, 4–7]. At the same time, low-Z organic materials showed high spin-transport coherence properties, making possible the integration of the spin degree of freedom in organics-based semiconductor devices [2, 8]. For both aspects the interface between the magnetically-active constituents has been shown to have a crucial impact [9–15].

Organic magnets were first reported for large-spin molecules such as $Mn_{12} - ac$ [16]. More recently the use of smaller, π -conjugated macrocycles such as phthalocyanines and porphyrins hosting a single transition metal atom has shown great versatility [9, 13–15, 17]. This includes, for instance, the possibility to modify the magnetic spin state of the central metal atom through ferromagnetic (FM) coupling to the substrate [13, 14, 18] or by further adsorption of smaller molecules [19, 20]. π -conjugated molecules are robust and can incorporate any transition metal. On the other hand they tend to organize via weak intermolecular bonding (van der Waals or H-bonding) thus limiting the possibility of designing new architectures at the nanoscale.

Currently an alternative approach for the synthesis of magneto-organic nanostructures is being explored. It consists in manipulating the magnetic properties of transition metal atoms through selective bonding to functional ligands in surface-supported, self-assembled metal-

organic networks [3, 21, 22]. Recent studies have shown that the magnetic coupling between metal centers, as well as their magnetic anisotropy, can be controlled by changing the nature of the metal-ligand (M-L) bonding or by adsorption of molecular oxygen [3, 21, 22].

Significantly, two recent studies have revealed FM coupling between magnetic centers in 2D organic self-assembled M-L networks [21, 22]. In both cases a superexchange coupling was suggested. For Fe-T4PT/Au(111) spin-density oscillations across ligands propagated through the network [21, 23]. In the case of Ni-TCNQ the measured FM coupling for adsorption on Au(111) is ascribed to favorable M-L charge transfer whereas for Ag(100) the participation of the substrate in the M-L interaction quenches the long range order [22].

In this context, the present study on the electronic structure and magnetic properties of a new M-L network, namely Mn coordinated with 1,2,4,5-tetracyanobenzene (Mn-TCNB) should bring a new piece of information for a comprehensive understanding of magnetic phenomena in organic M-L networks.

TCNB has raised interest recently for its potential ability to undergo a chemical reaction and form phthalocyanine derivatives or polymeric phthalocyanine [24, 25]. The choice of the Mn is also important in view of total spin and magnetic anisotropy properties. A large anisotropy is necessary for magnetic memory applications whereas small values open the way to qubit manipulation [26]. Mn with five d -electrons is a preferred candidate as a spin center in M-L networks. Under the action of organic ligands the presence of intra-molecular exchange interaction and sizable single-ion anisotropy were found [27–29] making Mn-based organic molecules suitable for single-molecule magnetism. Recently, detailed structural and

electronic studies on Mn-based M-L networks have been reported showing a rich interplay between metal centers, ligands and different substrates [30, 31], thus suggesting the possibility of finely tuning the Mn magnetic properties.

In the present paper, scanning tunneling microscopy (STM) was used to study the structure of the Mn-TCNB M-L network grown on two different substrates, namely Au(111) and Ag(111). Chemically and magnetically sensitive X-ray magnetic circular dichroism (XMCD [32]) in combination with multiplet calculations was used to study the effect of the M-L bonding on the Mn magnetic properties.

EXPERIMENT

The experiments were performed at the DEIMOS beamline, SOLEIL, France: it is an undulator beamline working in the soft-ray range with variable polarization. The end station houses a UHV sample preparation facility comprising sputtering and annealing for substrate preparation, molecular sublimation, STM and Auger electron spectroscopy (AES). Au(111) and Ag(111) surfaces were prepared by repeated cycles of sputtering and annealing. Subsequently a single layer of TCNB was deposited by sublimating the molecules from a crucible while keeping the substrate at room temperature. Finally, additional sublimation of Mn atoms resulted in the formation of the Mn-TCNB M-L network domains with a given stoichiometry. The Au(111) sample was post-annealed at 100° C for 10 minutes to increase the homogeneity of the network. Every step of the procedure was monitored by STM and AES. The STM images of Fig.1 were obtained at IM2NP in Marseille in equivalent experimental conditions.

X-ray absorption spectroscopy (XAS) with variable polarization was performed in total electron yield. XMCD is the difference between XAS spectra acquired with circularly polarized light, with opposite alignment of X-ray helicity vector (99% circularly polarized light) and sample magnetization. The spectra were taken at 3 K and under a magnetic field of 6 T applied along the light propagation direction. Measurements were performed at normal incidence (NI, $\Theta = 0^\circ$, Θ being the angle between the surface normal and the light beam) and at grazing incidence (GI, $\Theta = 70^\circ$). XMCD was also used to record magnetization curves by scanning the magnetic field and measuring the difference between resonance and off-resonance XAS at each step. The signal was then normalized to the XAS signal at the highest applied magnetic field. The final curves are the average of four magnetic field scans performed after changing either the X-ray helicity and the magnetic field. All the magnetization curves have been normalized for comparison with a model Brillouin function. A

least-squared fit to mean field theory spin Hamiltonian containing zero-field splitting and FM coupling terms was performed.

MULTIPLY CALCULATIONS

The XMCD spectra were calculated in the framework of the ligand field multiplet. A numerical code was developed which diagonalized the microscopic Hamiltonian in the initial ($2p^63d^5$) and final ($2p^53d^6$) configurations [51] and then computed the dipole transitions. The microscopic Hamiltonian of the p and d many-electron system

$$H = H_C + H_{SO} + H_{LF} + H_Z \quad (1)$$

contains, respectively, Coulomb repulsion in the d -shell and between p - and d -shells, spin-orbit interaction for p - and d -electrons, ligand field and Zeeman interaction with an external magnetic field.

Considering a D_{4h} symmetry for the Mn^{2+} environment, the ligand field is defined by D_q , D_s and D_t one-electron parameters. The last two give the deviation from a octahedral symmetry, characterized by $D_q > 0$. The ligand field Hamiltonian defines the four-fold z axis. The external magnetic field is defined by its magnitude B and the θ angle it makes with the z -axis (within the (x, z) plane).

All these parameters being set, H is diagonalized in initial (252 states) and final (1260 states) configurations under saturating magnetic field, resulting in a set of eigenvalues and eigenvectors. Subsequently, the absorption spectra are calculated considering dipole-allowed transitions with circularly-polarized light. The resulting spectra are broadened by a lorentzian function to take into account the finite lifetime of the core-hole.

RESULTS AND DISCUSSION

The STM images of Fig. 1 show the Mn-TCNB networks formed after sequential deposition of TCNB and Mn. On Au(111) the domains are more extended (40 to 50 nm) than for Ag(111) (about 20 nm). The unit cell is square with a 1.2 ± 0.1 nm periodicity and comprises two molecules and one metal atom for both substrates thus representing a $Mn(TCNB)_2$ stoichiometry. The corresponding schematic model of Fig. 1-d shows that each Mn atom is linked to 4 TCNB molecules through a Mn-N metal-ligand bonding displaying D_{4h} symmetry.

In Fig. 2 the XAS and XMCD spectra over the Mn $L_{3,2}$ edge are displayed for the two samples with the X-ray beam at different incidence angles. Despite the differences due to substrate background contributions the

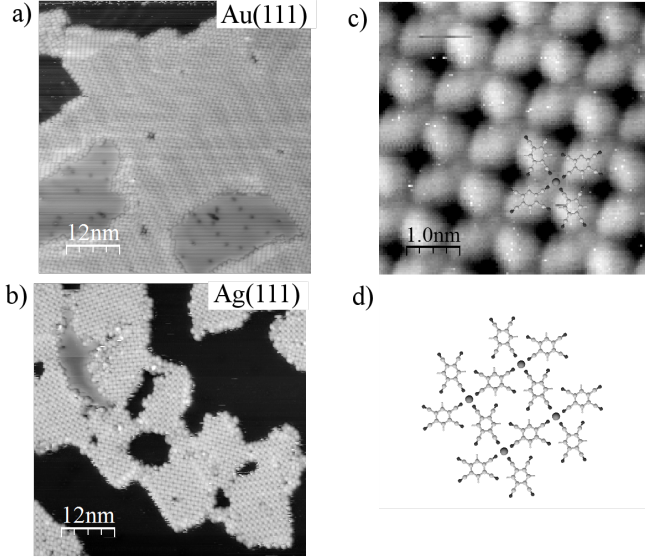


FIG. 1: STM images of Mn-TCNB networks formed after deposition on (a) Au(111) (b) and Ag(111). (d) High magnification image of the metal-organic structure on Au(111). (c) Ball-stick model of the network.

overall shape of the XAS spectra are similar for the two systems: both exhibit the spectral features typical of Mn^{2+} with a d^5 configuration.[3, 27–29, 33–41]. For both systems a clear difference is observed at the L_3 in going from NI to GI indicating a preferred orbital orientation.

The XMCD also displays anisotropy for both systems, more markedly at the L_3 . In NI a negative-positive pre-edge is followed by a strong but featureless negative peak (at 638.9 and 639.0 eV for Au and Ag respectively). In GI there is no clear pre-edge feature, but the main negative peak (638.8 and 638.9 eV for Au and Ag respectively) has a shoulder at low energy side. Finally the main peak intensity is weaker at GI than at NI. At the L_2 the differences are smaller but it can be seen that the onset of the white line is shifted to lower energies in GI.

The XMCD spectra changes significantly in going from Au(111) to Ag(111) substrate. The first difference is the quoted shift of 0.1 eV to higher energy for both sample orientations. The second, more clearly noticeable aspect, is that on Ag(111) the shoulder at the main negative peak in GI is more pronounced than on Au(111) and the GI to NI difference of peak height is more marked. Finally the onset shift at the L_2 is larger for Ag(111).

The magnetization curves for the two systems probed along the surface normal (NI) and close to sample surface plane (GI) are displayed in Fig. 3. For Mn-TCNB/Au(111) a small in-plane magnetic anisotropy is detected. Both curves are close to the Brillouin function for a $S = 5/2$ system at 3 K. The same kind of anisotropy is measured for Mn-TCNB adsorbed on Ag(111). Remarkably, for Ag(111) a clear departure from the Brillouin function is observed suggesting a FM cou-

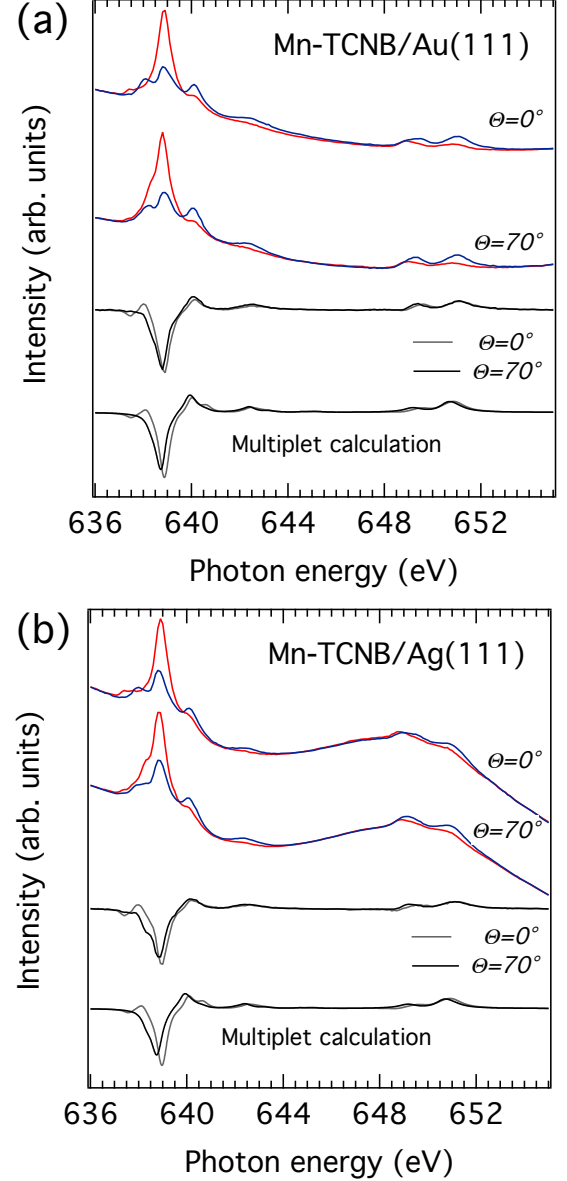


FIG. 2: Angular dependence of the XAS and resulting XMCD over the Mn $L_{2,3}$ edge for (a) Mn-TCNB/Au(111) and (b) Mn-TCNB/Ag(111) measured at 3K with an applied magnetic field of 6T parallel (blue) and antiparallel (red) to the X-ray beam helicity. Two sample orientations with respect to the light propagation direction were measured ($\Theta = 0^\circ$ correspond to normal incidence (NI) and $\Theta = 70^\circ$ to grazing incidence (GI)). The bottom curves are obtained by ligand field multiplet calculations (see text).

pling [21, 22]. The anisotropy observed for both systems indicates an easy plane parallel to the network plane.

In order to get more insight into the physical parameters governing the shape of the measured curves, we used a spin Hamiltonian with zero-field splitting (parameter D) and magnetic coupling between individual spins. This

was done in the framework of mean field theory, where the magnetic interaction of a spin with all other spins is replaced by an effective mean magnetic field \mathbf{B}_{eff} added to the external applied field \mathbf{B}_{ext} and proportional to the mean magnetization \mathbf{S}

$$H_S = DS_z^2 - g\mu_B \mathbf{B} \cdot \mathbf{S} \quad (2)$$

where $\mathbf{B} = \mathbf{B}_{\text{ext}} + \mathbf{B}_{\text{eff}}$ and $\mathbf{B}_{\text{eff}} = \lambda \mathbf{S}$. The Curie temperature associated with the magnetic coupling is given by $T_c = \lambda S(S+1)g\mu_B/(3k_B)$ [42]. The strength of the coupling is related to the Curie temperature as $T_c = \sum_i J_i/(3k_B)$, where the sum goes over the first 4 neighboring sites of the square Mn-lattice. In fact, the magnetic field includes also a contribution of the local field created by dipolar interaction of all surrounding spins:

$$\mathbf{B} = \mathbf{B}_{\text{ext}} + \mathbf{B}_{\text{eff}} + \mathbf{B}_{\text{dipol}} \quad (3)$$

For an infinite 2D square spin lattice of size a_0 , $\mathbf{B}_{\text{dipol}}$ is of the order of $(8\pi/3a_0^3)g\mu_B \mathbf{S}$ [43] and is about one order of magnitude smaller than the effective field \mathbf{B}_{eff} due to magnetic interaction. Note that both zero-field splitting and magnetic interaction terms are necessary to obtain a reasonable fit to the experimental data.

The experimental curves are fitted by the model with the following parameters (see supplementary information for details): $D = 0.015$ meV and $T_c = 0.3$ K ($J_i = 0.02$ meV) for Au(111); $D = 0.021$ meV and $T_c = 1.1$ K ($J_i = 0.07$ meV) for Ag(111). The sign of the anisotropy parameter indicates an easy-plane uniaxial anisotropy for both systems. The anisotropy energy is similar but the coupling is sensibly stronger for the Ag(111) substrate.

The zero-field splitting (or single-ion anisotropy) energy results from the combined effect of the ligand field acting on the Mn atoms and the atomic $d-d$ spin-orbit interaction. Because these parameters affect the XMCD their approximate values can be inferred by comparing the experiment to parameter-dependent model spectra. XMCD spectra with varying ligand field parameters were therefore calculated. The best agreement was obtained when $10D_q = 0.7$ eV and $D_t = 0.07$ eV for both substrates and $D_s = 0.07$ eV and $D_s = 0.10$ eV for Au(111) and Ag(111), respectively. The calculated spectra are displayed in the bottom parts of Figs. 2(a) and 2(b). The overall agreement of the simulations is satisfactory. All main experimental features are well reproduced in terms of energy and intensity. Namely the negative-positive pre-edge is present in the NI but absent in GI where a single negative peak is found instead. When Au(111) is changed to Ag(111) a higher D_s is found. This has several effects on the simulated spectra: (i) in GI a shoulder to the main negative peak develops at low energy; (ii) the difference in intensity at the main peak between GI and NI increases; (iii) at the L_2 the onset shift becomes larger. All these features allow to correctly reproduce

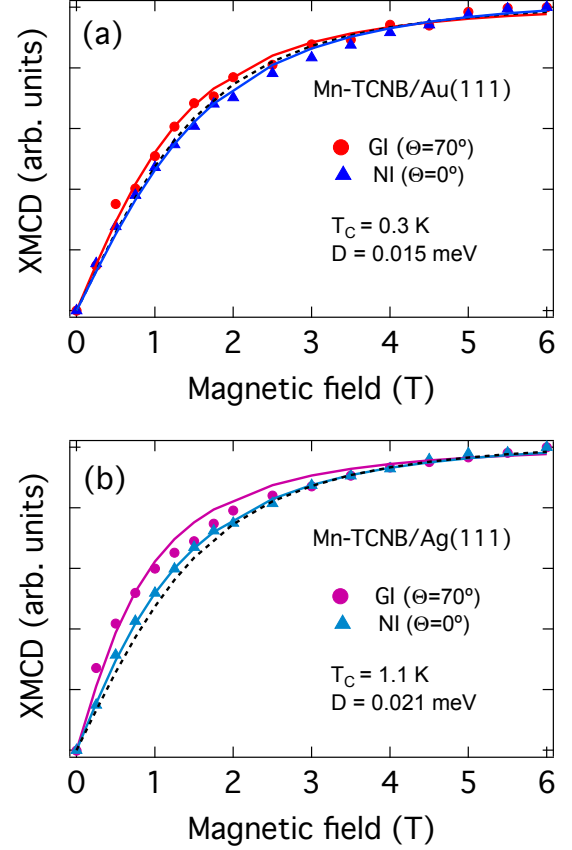


FIG. 3: Magnetization curves (symbols) as obtained from XMCD of (a) Mn-TCNB/Au(111) and (b) Mn-TCNB/Ag(111) at 3 K in NI and GI geometries. Superimposed (continuous lines) are the least-squared fitting curves obtained through equation (2) (see text for details). The resulting fitting parameters for the two systems are indicated. The Brillouin function at 3K is shown for comparison as a dashed line.

the main differences between the experimental spectra relative to Au and Ag substrates. Improvements in the agreement with the experimental spectra are expected to be obtained by using a more realistic electronic structure, including charge transfer effects and molecule-substrate interactions [9].

Even without such refinements the ligand field parameter sets can be used to calculate D by means of the microscopic Hamiltonian. This was done analytically by exactly solving the Coulomb operator H_C in the initial configuration ($\equiv d^5$) and then treating H_{SO} and H_{LF} as perturbations to the ground sextet (6S) energy. The results is to split this sextet into three pseudo-spin doublets ($|\tilde{m}_S\rangle = |\pm 5/2\rangle, |\pm 3/2\rangle, |\pm 1/2\rangle$ from highest to lowest lying) separated by $4D$ and $2D$, respectively. Similarly to the case of Mn^{2+} in C_{3v} symmetry [44], the fourth order expression of axial anisotropy for a d^5 configuration in D_{4h} symmetry is derived [52] :

$$D^{(4)} = \frac{63}{10} \frac{\zeta_d^2 D_s}{\mathcal{P}^2 \mathcal{D}} (\zeta_d - \frac{D_s}{3}) + 35 \frac{\zeta_d^2 D_t}{\mathcal{P}^2 \mathcal{G}} (2D_q - D_t) \quad (4)$$

where $\mathcal{P} = 7(\mathcal{B} + \mathcal{C})$, $\mathcal{D} = 17\mathcal{B} + 5\mathcal{C}$ and $\mathcal{G} = 10\mathcal{B} + 5\mathcal{C}$ are, respectively, the energy difference between the ground state sextet 6S and excited quartets of the d^5 configuration lying just above in energy: 4G , 4P and 4D . \mathcal{B} and \mathcal{C} are the Racah parameters, related to the Slater-Condon's by $F_{dd}^2 = 49\mathcal{B} + 7\mathcal{C}$ and $F_{dd}^4 = 63\mathcal{C}/5$. This formula relates one-electron ligand field (electric field plus hybridization) anisotropy parameters (D_q , D_t and D_s) to the magnetic anisotropy parameter (D) of a $S = 5/2$. (4) is thus very important to predict the effect of a modified chemical environment on the magnetic anisotropy properties.

When using $\zeta_d = 0.052$ eV, the resulting value of D is 0.012 meV and 0.011 meV for Au and Ag respectively. Such values are somehow smaller than those obtained by fitting the magnetization curves (for Au and Ag 0.015 meV and 0.021 meV, respectively). Nevertheless they confirm the presence of the single ion, easy-plane, uniaxial anisotropy [53]. Moreover, from (4) it results that although the in-plane tetragonal distortion D_s affects the angular dependence of the XMCD spectrum (of course in combination with D_t), it only has a weak influence on the anisotropy energy which is determined mainly by D_q and D_t through the spin-orbit interaction and is therefore very similar for the two substrates.

The results reported above indicate that within the Mn-TCNB M-L network, magnetic anisotropy is induced by the joint effect of ligand field and spin-orbit interaction. Comparatively, the zero-field splitting reported recently for high-spin, d^5 Mn in a star-shaped heteronuclear complex ($Cr^{III}Mn_3^{II}$) is as high as 0.124 meV [28]. On the other hand the magnetic coupling constant found here is higher than reported for star-shaped molecules having shorter Mn-Mn distance [28, 29]. This may be due to the extended two-dimensional character of the present system and to the presence of the metallic substrate, favoring delocalization of magnetic excitations.

Concerning the mechanism driving the magnetic coupling, previous FM behavior on 2D organic M-L networks was ascribed to superexchange interaction [21, 22]. Superexchange may also be the driving interaction in the case of Mn-TCNB. In such a perspective it should be noticed that for the Ag-supported system the D_s obtained from the XMCD simulation is higher than for Au. This may arise from a more effective M-L linkage resulting in a stronger magnetic coupling.

Notwithstanding the coupling mechanisms suggested in the previous studies of organic M-L networks are probably not adapted to explain the behavior encountered here. In fact, for Mn-TCNB the number of linker atoms between each Mn is even and thus a superexchange in-

teraction through spin density oscillation should be AFM [23]. A charge-state dependent coupling as observed for Ni-TCNQ [22] is not observed for Mn-TCNB where XAS spectra reveal that the charge state of the Mn atoms is the same on both substrates.

Conversely, for the present systems a substrate mediated FM coupling can be envisaged through Ruderman-Kittel-Kasuya-Yosida (RKKY) interactions [45]. In fact, above (111) noble metal surfaces collective screening occurs through the Shockley state and, to a first approximation, the key parameter determining the sign of the exchange interaction is the product of the lattice constant and the Fermi wave vector (k_F). Using the expression for RKKY interactions in 2D [46] one observes that the relatively small k_F of Ag(111) favors FM coupling between nearest neighbors (placed 1.2 nm apart). On the other hand, for Au(111) the two Rashba-split Shockley states have larger k_F values and at 1.2 nm distance the first minimum for the RKKY interaction is reached, resulting in a moderate AFM coupling. Certainly the real situation is more complex than the above scenario. Nevertheless, in a picture in which RKKY would compete with other channels of magnetic coupling (such as superexchange as mentioned earlier), the FM to AFM screening in going from Ag(111) to Au(111) may help to explain the differences measured in the magnetization curves of the two otherwise very similar Mn-TCNB networks. It would be interesting to test such a scenario for Ag(100) substrate where the surface states are unoccupied and no long-range oscillation of the exchange interactions is expected [47].

CONCLUSION

In summary, the structure and the magnetic properties of two Mn-TCNB metal-ligand networks were studied by STM and low-temperature XMCD. Angle-dependent magnetization curves show FM coupling between the equally spaced Mn atoms with in-plane uniaxial anisotropy. Ligand field multiplet calculations were used to simulate the experimental spectra. The obtained parameter values allow an estimation of the anisotropy energy, confirming the magnetization curves analysis. The spectroscopic differences between Mn-TCNB on Au(111) and Ag(111) indicate a stronger in-plane distortion of the ligand field for adsorption on Ag(111). This may be the result of a stronger metal-ligand interaction favoring superexchange coupling. Another possible explanation for the different magnetic coupling between Ag(111) and Au(111) is given in terms of RKKY interaction. Because M-L networks are versatile extended 2D systems in which the inter-atomic distance is controlled by the choice of the organic linkers, in the future they may emerge as a new approach to the study of surface

magnetic screening phenomena beside single atom manipulation [48] and self assembly of π -conjugated molecules containing magnetic centers [45]. Finally, an expression (4) is given for the magnetic anisotropy energy of a d^5 configuration in a D_{4h} environment as a function of crystal field parameters. This should be seen as a helpful tool to predict, and possibly tune, the magnetic anisotropy properties via organic linkers. A future development of the model will focus on the magnetic coupling, possibly including hybridization and surface-mediated interactions.

ACKNOWLEDGMENTS

The preparation chambers of the DEIMOS beam line have been partially funded by the Agence National de la Recherche (grant ANR-05-NANO-073).

SUPPLEMENTARY INFORMATION

The spin Hamiltonian (2) was solved to calculate the average magnetization vector \mathbf{M} depending on the applied field \mathbf{B} . However, due to the zero-field splitting term, \mathbf{M} and \mathbf{B} are in general not aligned (except when \mathbf{B} is applied along the easy-plane). The experimental XMCD signal is only sensitive to the projection of \mathbf{M} along the direction of the X-rays (which is in our case identical to the direction of the applied field \mathbf{B} , see Fig. S4). Furthermore, it also accounts for a magnetic dipole operator term, the angle dependence of which can be approximated to $(1 - 3 \cos(2\Theta_M))$ [17, 21] (Fig. S4). As a result, the XMCD intensity was calculated as

$$I_{XMCD} = A \cos(\Theta_M - \Theta_B) |M| (1 - C(1 - 3 \cos(2\Theta_M))) \quad (5)$$

Where A is a normalization factor and C accounts for the strength of the magnetic dipole moment (the latter was very small in the present case due to the spherical symmetry of $d^5 Mn^{II}$ [49]). For every set of D and T_c , the parameters A and C are simultaneously tuned to minimize the total mean squared deviation for grazing and normal incidence of the calculated curves with respect to the experimental data. The resulting deviations are reported in Fig. S5 for the Au(111) and Ag(111) substrates. In both cases, a clear minimum is found.

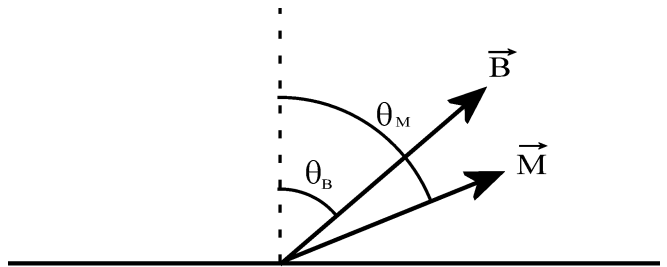


FIG. 4: Schematic of relative orientations of \mathbf{B} and \mathbf{M} . The angles are relative to the surface normal (magnetic hard axis). The direction of the X-ray beam is aligned with the applied magnetic field.

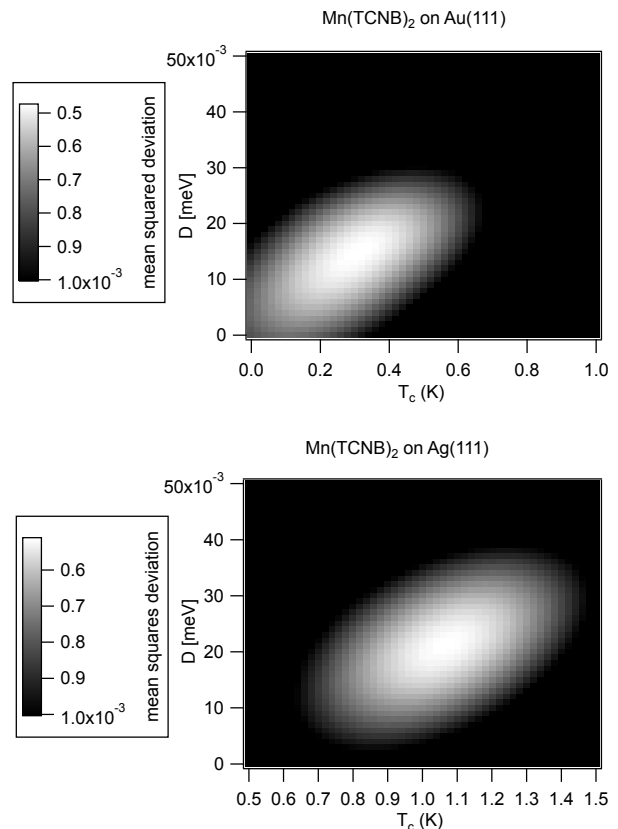


FIG. 5: Mean squared deviation of the simulated magnetization curves with respect to the experimental data calculated for the two substrates. The black regions correspond to deviations $\geq 10^3$. The best fit is obtained with $D=0.015$ meV and $T_c=0.3$ K for Au(111), and $D=0.021$ meV and $T_c=1.1$ K for Ag(111)

- [1] T. Miyamachi, M. Gruber, V. Davesne, M. Bowen, S. Boukari, L. Joly, F. Scheurer, G. Rogez, T. K. Yamada, P. Ohresser, et al., Nat Commun **3**, 1 (2012).
- [2] S. Sanvito, Chem. Soc. Rev. **40**, 3336 (2011).

- [3] P. Gambardella, S. Stepanow, A. Dmitriev, J. Honolka, F. M. F. de Groot, M. Lingenfelder, S. S. Gupta, D. D. Sarma, P. Bencok, S. Stanesco, et al., Nat Mater **8**, 189 (2009).
- [4] P. Ghigna, A. Campana, A. Lascialfari, A. Caneschi, D. Gatteschi, A. Tagliaferri, and F. Borgatti, Phys. Rev.

- B **64**, 132413 (2001).
- [5] C. Schlegel, J. van Slageren, M. Manoli, E. K. Brechin, and M. Dressel, *Phys. Rev. Lett.* **101**, 147203 (2008).
 - [6] M. Mannini, F. Pineider, P. Saintavit, C. Danieli, E. Otero, C. Sciancalepore, A. M. Talarico, M.-A. Arrio, A. Cornia, D. Gatteschi, et al., *Nat Mater* **8**, 194 (2009).
 - [7] S. Stepanow, J. Honolka, P. Gambardella, L. Vitali, N. Abdurakhmanova, T.-C. Tseng, S. Rauschenbach, S. L. Tait, V. Sessi, S. Klyatskaya, et al., *Journal of the American Chemical Society* **132**, 11900 (2010).
 - [8] K. V. Raman, A. M. Kamerbeek, A. Mukherjee, N. Atodiresi, T. K. Sen, P. Lazic, V. Caciuc, R. Michel, D. Stalke, S. K. Mandal, et al., *Nature* **493**, 509 (2013).
 - [9] S. Stepanow, P. S. Miedema, A. Mugarza, G. Ceballos, P. Moras, J. C. Cezar, C. Carbone, F. M. F. de Groot, and P. Gambardella, *Phys. Rev. B* **83**, 220401 (2011).
 - [10] S. Sanvito, *Nature Physics* **6**, 562 (2010).
 - [11] S. Javai, M. Bowen, S. Boukari, L. Joly, J.-B. Beaufrand, X. Chen, Y. J. Dappe, F. Scheurer, J.-P. Kappler, J. Arabski, et al., *Phys. Rev. Lett.* **105**, 077201 (2010).
 - [12] H. Wende, M. Bernien, J. Luo, C. Sorg, N. Ponpandian, J. Kurde, J. Miguel, M. Piantek, X. Xu, P. Eckhold, et al., *Nat Mater* **6**, 516 (2007).
 - [13] E. Annese, J. Fujii, I. Vobornik, G. Panaccione, and G. Rossi, *Phys. Rev. B* **84**, 174443 (2011).
 - [14] E. Annese, F. Casolari, J. Fujii, and G. Rossi, *Phys. Rev. B* **87**, 054420 (2013).
 - [15] P. Gargiani, G. Rossi, R. Biagi, V. Corradini, M. Pedio, S. Fortuna, A. Calzolari, S. Fabris, J. C. Cezar, N. B. Brookes, et al., *Phys. Rev. B* **87**, 165407 (2013).
 - [16] L. Thomas, F. Lioni, R. Ballou, D. Gatteschi, R. Sessoli, and B. Barbara, *Nature* **383**, 145 (1996).
 - [17] S. Stepanow, A. Mugarza, G. Ceballos, P. Moras, J. C. Cezar, C. Carbone, and P. Gambardella, *Phys. Rev. B* **82**, 014405 (2010).
 - [18] M. Bernien, J. Miguel, C. Weis, M. E. Ali, J. Kurde, B. Krumme, P. M. Panchmatia, B. Sanyal, M. Piantek, P. Srivastava, et al., *Phys. Rev. Lett.* **102**, 047202 (2009).
 - [19] C. Wäckerlin, D. Chylarecka, A. Kleibert, K. Müller, C. Iacovita, F. Nolting, T. A. Jung, and N. Ballav, *Nature Communications* **1**, 61 (2010).
 - [20] C. Isvoranu, B. Wang, K. Schulte, E. Ataman, J. Knudsen, J. N. Andersen, M. L. Bocquet, and J. Schnadt, *Journal of Physics: Condensed Matter* **22**, 472002 (2010).
 - [21] T. R. Umbach, M. Bernien, C. F. Hermanns, A. Krüger, V. Sessi, I. Fernandez-Torrente, P. Stoll, J. I. Pascual, K. J. Franke, and W. Kuch, *Phys. Rev. Lett.* **109**, 267207 (2012).
 - [22] N. Abdurakhmanova, T.-C. Tseng, A. Langner, C. S. Kley, V. Sessi, S. Stepanow, and K. Kern, *Phys. Rev. Lett.* **110**, 027202 (2013).
 - [23] V. Bellini, G. Lorusso, A. Candini, W. Wernsdorfer, T. B. Faust, G. A. Timco, R. E. P. Winpenny, and M. Affronte, *Phys. Rev. Lett.* **106**, 227205 (2011).
 - [24] M. Abel, S. Clair, O. Ourdjini, M. Mossoyan, and L. Porte, *Journal of the American Chemical Society* **133**, 1203 (2011).
 - [25] D. M. Sedlovets, M. V. Shuvalov, Y. V. Vishnevskiy, V. T. Volkov, I. I. Khodos, O. V. Trofimov, and V. I. Korepanov, *Materials Research Bulletin* **48**, 3955 (2013).
 - [26] S. Bertaina, L. Chen, N. Groll, J. Van Tol, N. S. Dalal, and I. Chiorescu, *Phys. Rev. Lett.* **102**, 050501 (2009).
 - [27] K. Kuepper, D. M. Benoit, U. Wiedwald, F. Mögele, A. Meyering, M. Neumann, J.-P. Kappler, L. Joly, S. Weidle, B. Rieger, et al., *J. Phys. Chem. C* **115**, 25030 (2011).
 - [28] M. Prinz, K. Kuepper, C. Taubitz, M. Raekers, S. Khanra, B. Biswas, T. Weyhermüller, M. Uhlarz, J. Wosnitza, J. Schnack, et al., *Inorganic Chemistry* **49**, 2093 (2010).
 - [29] S. Khanra, K. Kuepper, T. W. , M. Prinz, M. Raekers, S. Voget, A. V. Postnikov, F. M. F. de Groot, S. J. George, M. Coldea, et al., *Inorganic Chemistry* **47**, 4605 (2008).
 - [30] T.-C. Tseng, C. Lin, X. Shi, S. L. Tait, X. Liu, U. Starke, N. Lin, R. Zhang, C. Minot, M. A. Van Hove, et al., *Phys. Rev. B* **80**, 155458 (2009).
 - [31] M. N. Faraggi, N. Jiang, N. Gonzalez-Lakunza, A. Langner, S. Stepanow, K. Kern, and A. Arnau, *The Journal of Physical Chemistry C* **116**, 24558 (2012).
 - [32] J. Stöhr, *Journal of Magnetism and Magnetic Materials* **200**, 470 (1999).
 - [33] M.-A. Arrio, P. Saintavit, C. Cartier dit Moulin, T. Malah, M. Verdaguer, E. Pellegrin, and C. T. Chen, *Journal of the American Chemical Society* **118**, 6422 (1996).
 - [34] Y. Nanba and K. Okada, *Journal of Electron Spectroscopy and Related Phenomena* **185**, 167 (2012).
 - [35] P. Gambardella, L. Claude, S. Rusponi, K. J. Franke, H. Brune, J. Raabe, F. Nolting, P. Bencok, A. T. Hanbicki, B. T. Jonker, et al., *Physical Review B* **75**, 125211 (2007).
 - [36] M. Nagel, I. Biswas, P. Nagel, E. Pellegrin, S. Schuppler, H. Peisert, and T. Chassé, *Phys. Rev. B* **75**, 195426 (2007).
 - [37] J.-S. Kang, G. Kim, H. J. Lee, D. H. Kim, H. S. Kim, J. H. Shim, S. Lee, H. Lee, J.-Y. Kim, B. H. Kim, et al., *Phys. Rev. B* **77**, 035121 (2008).
 - [38] K. W. Edmonds, G. van der Laan, A. A. Freeman, N. R. S. Farley, T. K. Johal, R. P. Campion, C. T. Foxon, B. L. Gallagher, and E. Arenholz, *Phys. Rev. Lett.* **96**, 117207 (2006).
 - [39] F. Maccherozzi, M. Sperl, G. Panaccione, J. Minár, S. Polesya, H. Ebert, U. Wurstbauer, M. Hochstrasser, G. Rossi, G. Woltersdorf, et al., *Phys. Rev. Lett.* **101**, 267201 (2008).
 - [40] S. P. Cramer, F. M. F. DeGroot, Y. Ma, C. T. Chen, F. Sette, C. A. Kipke, D. M. Eichhorn, M. K. Chan, and W. H. a. Armstrong, *Journal of the American Chemical Society* **113**, 7937 (1991).
 - [41] F. M. F. de Groot, J. C. Fuggle, B. T. Thole, and G. A. Sawatzky, *Phys. Rev. B* **42**, 5459 (1990).
 - [42] N. W. Ashcroft and N. D. Mermin, *Solid State Physics* (Harcourt, 1976).
 - [43] Y. Yafet and E. M. Gyorgy, *Phys. Rev. B* **38**, 9145 (1988).
 - [44] A. Savoyant, A. Stepanov, R. Kuzian, C. Deparis, C. Morhain, and K. Grasz, *Phys. Rev. B* **80**, 115203 (2009).
 - [45] N. Tsukahara, S. Shiraki, S. Itou, N. Ohta, N. Takagi, and M. Kawai, *Phys. Rev. Lett.* **106**, 187201 (2011).
 - [46] B. Fischer and M. W. Klein, *Phys. Rev. B* **11**, 2025 (1975).
 - [47] E. Simon, B. Újfalussy, B. Lazarovits, A. Szilva, L. Szunyogh, and G. M. Stocks, *Phys. Rev. B* **83**, 224416 (2011).
 - [48] A. A. Khajetoorians, J. Wiebe, B. Chilian, S. Lounis,

- S. Blugel, and R. Wiesendanger, Nat Phys **8**, 497 (2012).
- [49] J. P. Crocombette, B. T. Thole, and F. Jollet, Journal of Physics: Condensed Matter **22**, 4095 (1996).
- [50] E. Stavitski and F. M. de Groot, Micron **41**, 687 (2010).
- [51] The Hartree-Fock energies reduced to 80% of the atomic values as obtained from the CTM4XAS program [50] were used
- [52] When calculating the energies of $H = DS_z^2$ for a spin 5/2 (six states) one finds 3 doublets separated by 2D and 4D (giving 6D between the lowest and the highest). The perturbative calculation of level 6S gives exactly 3 doublets separated by the same ratio, which allows to assign them to those of an effective 5/2 spin under the action of $H = DS_z^2$. It should be noticed that the expression for D is equally valid for the following symmetries: D_4 , D_{2d} and C_{4v}
- [53] It has to be stressed out that values of D closer to those obtained from fitting the magnetization curves can be obtained through (4) by further increasing the spin-orbit parameter ζ and without altering the simulated XMCD spectrum appreciably. Nevertheless, a free ion value was chosen since ζ is known to be *reduced* by the effect of the environment